Possible pairing states of the Fe-based superconductors

Yunkyu Bang*
Department of Physics, Chonnam National University, Kwangju 500-757, Republic of Korea
and Asia Pacific Center for Theoretical Physics, Pohang 790-784, Republic of Korea

Han-Yong Choi
Department of Physics and Institute for Basic Science Research, SungKyunKwan University, Suwon 440-746, Republic of Korea
(Received 25 July 2008; published 17 October 2008)

We consider the minimal two-band model for the Fe-based superconductors with a phenomenological pairing interaction which mimics short-range antiferromagnetic fluctuations. Two superconducting (SC) gap solutions are found to exist with the model: sign-changing s-wave gap ($\pm s$ wave) and double d-wave gap states. Both solutions hold the approximate relation $\Delta_h^{\max} N_h \approx \Delta_e^{\max} N_e$, a generic feature of two-band model with a dominant interband pairing interaction. We carried out the calculations of the SC properties of the both SC states such as the density of states, temperature dependencies of spin-lattice relaxation rate $1/T_1$, Knight shift, and penetration depth, particularly taking into account of the interband coherence factors. The results are discussed in comparison with the currently available experimental data.

DOI: 10.1103/PhysRevB.78.134523 PACS number(s): 74.20.Rp, 74.20.De, 74.20.Mn

I. INTRODUCTION

Recent discovery of the Fe-based superconducting compounds provided a great impetus to the research of superconductivity (SC). Since the first report on the superconducting transition at 7 K with the doped LaOFeP by Kamihara *et al.*,[1] various substitutions (mainly P by As and La by Ce, Gd, Sm, and Pr) for this mother compound increase the superconducting temperature T_c over 50 K with Sm(OF)FeAs.[2] Intensive investigations by many experimentalists and theorists have already revealed main metallic and superconducting properties of this group of materials.

From band calculations,[3–8] it is agreed on that the 3d electrons of Fe atoms are the main contributors to the conduction bands crossing the Fermi surface (FS). Besides the degree of degeneracy, the key feature of conduction bands is that it consist of hole band(s) around Γ point and electron band(s) around M point [in the notation of the folded Brillouin-zone (BZ) scheme].[3,5]

Regarding the pairing symmetry, there are already many experiments: (1) Knight shift below T_c shows a clear drop indicating a spin singlet pairing;[9] (2) tunneling spectroscopy[10] showed the zero-bias conductance peak (ZBCP)—signature of a sign changing gap, but the interpretation of the shape of density of states (DOS) $N(\omega)$ is diverse; (3) nuclear-spin-lattice relaxation rate $1/T_1$ (Refs. 9 and 11) unanimously showed no coherent peak and $\sim T^3$ dependence below T_c, hence strongly suggesting a d-wave type gap; and (4) specific-heat coefficient $C(T)/T$ below T_c (Ref. 12)—although the measurement is not yet reaching low enough temperature—appears T linear indicating the gap with lines of node. All these experiments appear to be consistent with a d-wave-type gap. However, recent penetration depth measurements with PrFeAsO, Sm(OF)FeAs and Nd(OF)FeAs (Ref. 13) strongly suggest a fully opened gap at low temperatures indicating a s-wave-type pairing symmetry.

Regarding the paring glues, the phonon interaction appears unlikely mainly because the electron-phonon coupling is estimated to be very weak ($\lambda < 0.2$).[14] On the other hand, this series of materials, without doping, commonly has a spin-density wave (SDW) transition at around $\sim$150 K. When the superconductivity appears with doping, the SDW correlation is expected to remain albeit the long-range order disappears.

Recent neutron-scattering experiments with La(OF)FeAs and Ce(OF)FeAs (Ref. 15) directly measured the antiferromagnetic (AFM)-type correlation of the Fe d-electron-spin moment. The overall phase diagram with doping for Ce(OF)FeAs reveals a close correlation with an antiferromagnetism and superconductivity, suggesting the important role of magnetic fluctuations as a pairing glue. It also shows that the generic phase diagram of these compounds shares the universal features with the high-T_c cuprates, Pu-115 superconductor,[16] and various heavy fermion superconductors; namely, the SC occurs in the neighborhood of the magnetic long-range order when this magnetic order is suppressed. In particular, the magnetic order is an AFM type. This universal phase diagram is very tantalizing because it appears to cover a wide class of unconventional SC materials with a range of T_c from a few millikelvin to 100 K and suggests that the AFM fluctuation is a common thread and its characteristic energy roughly scales with the SC T_c.[16]

For the Fe-based SC materials, several theoretical models were already proposed and most of them started with the orbital basis of the Fe 3d electrons including Hubbard U interaction(s) and Hund coupling(s) J.[5,17–20] Some of these studies[5,17,18] found the $\pm s$-wave gap as a dominant instability. A d-wave gap also often appears as a second instability.[17,19] In this paper, we took a phenomenological approach to investigate possible pairing states in the Fe-pnitide superconductors. The noninteracting part of Hamiltonian is constructed by choosing a minimal set of topologically distinct two bands and the interaction part of Hamiltonian is assumed from the experimental input[15,21] simulating a short-range AFM correlation. By solving the coupled BCS gap equations, we found the two SC gap solutions: a sign-changing s-wave gap and a double d-wave gap. For the both SC states, we carried out the calculations of the

SC properties such as the DOS, temperature dependencies of the spin-lattice relaxation rate $1/T_1$, Knight shift, and penetration depth. We particularly take into account of the interband coherence factors, unique to the two-band model, in these calculations. The results are discussed in comparison with the currently available experimental data.

II. MODEL

We propose a minimal phenomenological two-band model for the Fe-based superconductors. For the noninteracting part of Hamiltonian, we observe that several band-structure calculations[3–8] of the Fe-pnictide compounds reached the consensus that the FS of the doped compounds consists of two hole pockets and two electron pockets. To keep the essential physics, but avoiding unnecessary complexity, we choose only two topologically distinct bands: one hole band around Γ point (0,0) and one electron band around M point $(\pm\pi, \pm\pi)$.

The main phenomenological assumption of our model is the interacting part of Hamiltonian. This pairing interaction $V(\mathbf{q})$ is chosen to simulate a short-range AFM spin fluctuations peaking at the ordering wave vector $\mathbf{Q}=(\pm\pi, \pm\pi)$. This assumption is directly motivated by the experimental observations of the AFM correlation in the Fe-pnictide compounds by the neutron-scattering measurements.[15,21] The elastic neutron-scattering experiments for $La(F_xO_{1-x})FeAs$ and $Ce(F_xO_{1-x})FeAs$ by Zhao and co-workers[15] showed the long-range AFM order of the Fe $3d$-electron spins for the doping range of $x=0-0.05$. When this long-range AFM order disappears beyond the doping around $x=0.05$, SC appears up to the doping range $x\sim 0.2$ (this is only the limit of the measured data). This overall phase diagram appears to be generic for the Fe pnictides and clearly shows that the AFM correlation is the dominant magnetic correlation in this group of materials.

More importantly, this AFM correlation is expected to continue to exist in the doping range where the SC phase occurs albeit becoming a short-range one. This speculation is supported by more recent inelastic neutron-scattering experiment in the doped $(BaK)Fe_2As_2$ compound ($T_c=38$ K) by Christianson *et al.*[21] In this experiment, a clear magnetic-resonance peak is observed at the expected position of the AFM correlation, i.e., at (π,π) momentum. With this series of experiments it is clear that the AFM correlation is the dominant magnetic correlation in the Fe pnictides among other competing magnetic correlations such as weak ferromagnetism,[3,4] checkerboard AFM,[8,6] and AFM stripe phase,[8,22] which were theoretically proposed. Finally, the coupling matrix element is assumed to be a constant for simplicity. The Hamiltonian is written as

$$H=\sum_{k\sigma}\varepsilon_h(k)h^\dagger_{k\sigma}h_{k\sigma}+\sum_{k\sigma}\varepsilon_e(k)e^\dagger_{k\sigma}e_{k\sigma}+\sum_{kk'\uparrow\downarrow}V(k,k')h^\dagger_{k\uparrow}h^\dagger_{-k\downarrow}h_{k'\downarrow}h_{-k'\uparrow}+\sum_{kk'\uparrow\downarrow}V(k,k')h^\dagger_{k\uparrow}h^\dagger_{-k\downarrow}e_{k'\downarrow}e_{-k'\uparrow}+\sum_{kk'\uparrow\downarrow}V(k,k')e^\dagger_{k\uparrow}e^\dagger_{-k\downarrow}h_{k'\downarrow}h_{-k'\uparrow}, \quad (1)$$

where $h^\dagger_{k\sigma}$ and $e^\dagger_{k\sigma}$ are the electron creation operators on the hole and the electron bands, respectively. $\varepsilon_{h,e}(k)$ are the dispersions of the hole band and electron bands, respectively, defined as $\varepsilon_h(k)=t^h_1(\cos k_x+\cos k_y)+t^h_2\cos k_x\cos k_y+\varepsilon^h$ and $\varepsilon_e(k)=t^e_1(\cos k_x+\cos k_y)+t^e_2\cos\frac{k_x}{2}\cos\frac{k_y}{2}+\varepsilon^e$. In this paper, we choose the band parameters as (0.30,0.24,–0.6) for hole band and (1.14,0.74,1.70) for electron band with the notation (t_1,t_2,ε).[18]

The pairing interaction $V(k,k')$ is phenomenologically defined below. It is all repulsive in momentum space and it represents a short-range AFM spin fluctuations as explained above.

$$V(k,k')=V_M\frac{\kappa^2}{|(\vec{k}-\vec{k}')-\vec{Q}|^2+\kappa^2}, \quad (2)$$

where $\vec{k}$ and $\vec{k}'$ are the two-dimensional momenta on the two-dimensional BZ and the parameter κ controls the magnetic correlation length as $\xi_{AFM}=2\pi a/\kappa$ (a is the unit-cell distance). This interaction mediates the strongest repulsion when two momenta $\vec{k}$ and $\vec{k}'$ are spanned by the ordering wave vector $\vec{Q}$. This condition is better fulfilled when the two momenta $\vec{k}$ and $\vec{k}'$ reside each other on different bands in the model band structure (see Fig. 1). As a result, the sign-changing s-wave gap can form on each band as already suggested by several papers.[5,17–19] However, this opposite sign gap on the hole and electron bands is not limited with the $\pm s$-wave state [Fig. 1(a)]. Another possibility, which conforms to the lattice symmetry, is that each band develops a d-wave gap but with π phase shift between two bands [Fig. 1(b)]. We call this type of gap as double d-wave gap.

We need to mention that our model did not include the screened Coulomb interaction (neither did the other theoretical investigations[5,17,19]), which certainly exists in the Fe-pnitide superconductors as well as in all metals in general. The screened Coulomb interaction is traditionally treated as "Coulomb pseudopotential" μ^* in the conventional phonon-driven SC. However, the reliable estimate for its strength is practically impossible because even a small difference in μ^* would cause a large change in T_c. In the Fe pnictides, if we are to determine T_c theoretically, a quantitative estimate of μ^* is necessary. We did not include it in our model interaction, first, because we do not know how to reliably estimate it in these compounds and, second, because the primary purpose of the present paper is not the prediction of the precise T_c. Still we could investigate its generic effects on the different pairing symmetries such as $\pm s$-wave and double d-wave gaps; for example, how large value of μ^* is necessary to kill the $\pm s$-wave pairing for a given strength of the AFM interaction. We think that this kind of analysis will dilute the focus of the present paper and therefore should be a separate investigation. We only briefly remark on the general effects of the screened Coulomb interaction. The

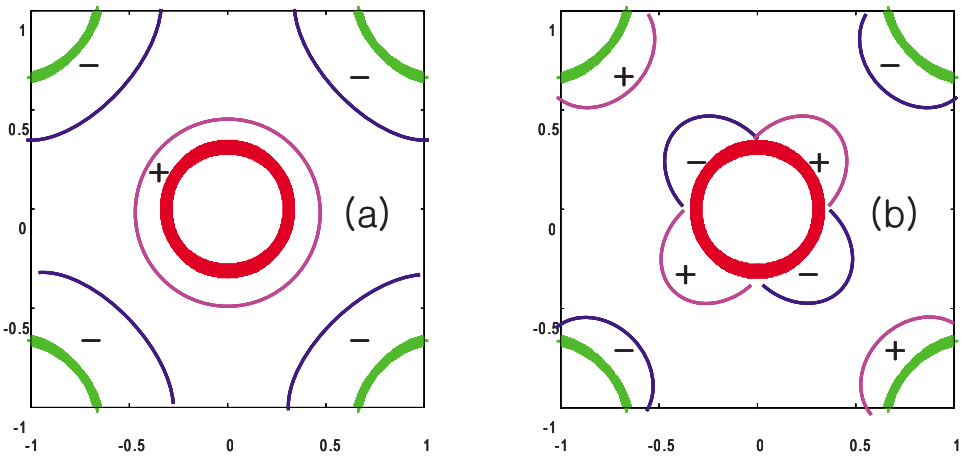

FIG. 1. (Color online) FSs of $\varepsilon_h(k)$ (red) and $\varepsilon_e(k)$ (green) bands and two gap solutions considered in the paper: (a) $\pm s$-wave gap and (b) double d-wave gap. The width of the FS represents the local DOS for each band within $\omega_{\mathrm{AFM}}=20$ meV energy.

screened Coulomb interaction becomes a short-range interaction in real space and therefore weakly momentum dependent in momentum space. This type of interaction is almost harmless for the d-wave-type pairing but extremely detrimental for the s-wave-type pairing. The pairing solutions in this paper should be considered with this point in mind.

Now we solve the Hamiltonian (1) using the BCS approximation and the two band electrons need two SC order parameters (OPs)

$$\Delta_h(k) = \sum_{k'} V(k,k')\langle h_{k'\downarrow} h_{-k'\uparrow}\rangle, \tag{3}$$

$$\Delta_e(k) = \sum_{k'} V(k,k')\langle e_{k'\downarrow} e_{-k'\uparrow}\rangle. \tag{4}$$

After decoupling the interaction terms of Eq. (1) using the above OPs, the self-consistent mean-field conditions lead to the following two coupled gap equations.

$$\Delta_h(k) = -\sum_{k'} [V_{hh}(k,k')\Delta_h(k')\chi_h(k') + V_{he}(k,k')\Delta_e(k')\chi_e(k')], \tag{5}$$

$$\Delta_e(k) = -\sum_{k'} [V_{eh}(k,k')\Delta_h(k')\chi_h(k') + V_{ee}(k,k')\Delta_e(k')\chi_e(k')], \tag{6}$$

where $V_{hh}(k,k')$, $V_{he}(k,k')$, etc. are the same interaction defined in Eq. (2) but the subscripts are written to clarify the meaning of $V_{hh}(k,k')=V(k_h,k'_h)$, $V_{he}(k,k')=V(k_h,k'_e)$, etc., and k_h and k_e specify the momentum k located on the hole and electron bands, respectively. The pair susceptibilities are defined as

$$\chi_{h,e}(k) = N(0)_{h,e}\int_0^{\omega_{\mathrm{AFM}}} d\xi \frac{\tanh\left(\frac{E_{h,e}(k)}{2T}\right)}{E_{h,e}(k)}, \tag{7}$$

where $E_{h,e}(k)=\sqrt{\xi^2+\Delta^2_{h,e}(k)}$ and $N(0)_{h,e}$ are the quasiparticle excitations and the DOS of the hole and electron bands, respectively, and ω_{AFM} is the cutoff energy of the pairing potential $V(q)$.

When we solve the above gap equations (5) and (6), we numerically restricted the momenta $k_{h,e}$ and $k'_{h,e}$ around the FSs of the hole and electron bands within ω_{AFM} energy range. Therefore, the FS shapes and the local DOS $N(0)_{h,e}$ of the realistic bands are faithfully taken into account in our gap solutions. Also no restriction on the functional forms of the gaps $\Delta_{h,e}(k)$ was imposed except the general symmetry depicted in Fig. 1, so that the k dependence of the gap functions $\Delta_{h,e}(k)$ will follow the characteristics of the bands and pairing interaction.

III. GAP SOLUTIONS

As explained in Sec. II, the main pairing process with the AFM spin-fluctuation-mediated interaction $V(q)$ is the interband pair hopping between the hole and the electron bands, in which a pair of electrons $(k,-k)$ on the hole band scatters to a pair of electrons $(k',-k')$ on the electron band and vice versa. This process is particularly dominant when the size of the FS of each band is much smaller than the size of $\vec{Q}$ vector. Considering only this interband pair process [keeping only V_{he} and V_{eh} terms in Eqs. (5) and (6)], we observe the fact that the pair potential $\Delta_h(k)$ for the hole band electrons is provided by the pairs of electrons in the electron band and vice versa. The physical consequence of it is that the relative sizes of the gaps and DOSs on each band are reversed; namely, if $N_h(0)>N_e(0)$, then $|\Delta_h(k)|<|\Delta_e(k)|$ holds in general. This relation holds both for the $\pm s$-wave and for the double d-wave gap solutions and affects all superconducting properties such as tunneling DOS, Knight shift $1/T_1$, and penetration depth.

For all numerical calculations in this paper, we choose the parameters $\kappa=0.2\pi$ ($\xi_{\mathrm{AFM}}\sim 10a$), $\omega_{\mathrm{AFM}}=20$ meV, and $V_M=10$ eV (average interaction $\langle V(q)\rangle=1.115$ eV). Our choice of band parameters produces $N_h(0)=0.74/\mathrm{eV}$ and $N_e(0)=0.285/\mathrm{eV}$, so that $N_h(0)/N_e(0)\approx 2.6$. We think that these numbers represent the Fe-based SC materials but should not be taken too seriously; in particular, the pairing strength $V_M=10$ eV is chosen freely for demonstration.

A. $\pm s$-wave gap

This solution for the Fe-based SC is already proposed by several authors.[5,17–19] Here we demonstrate that this solution

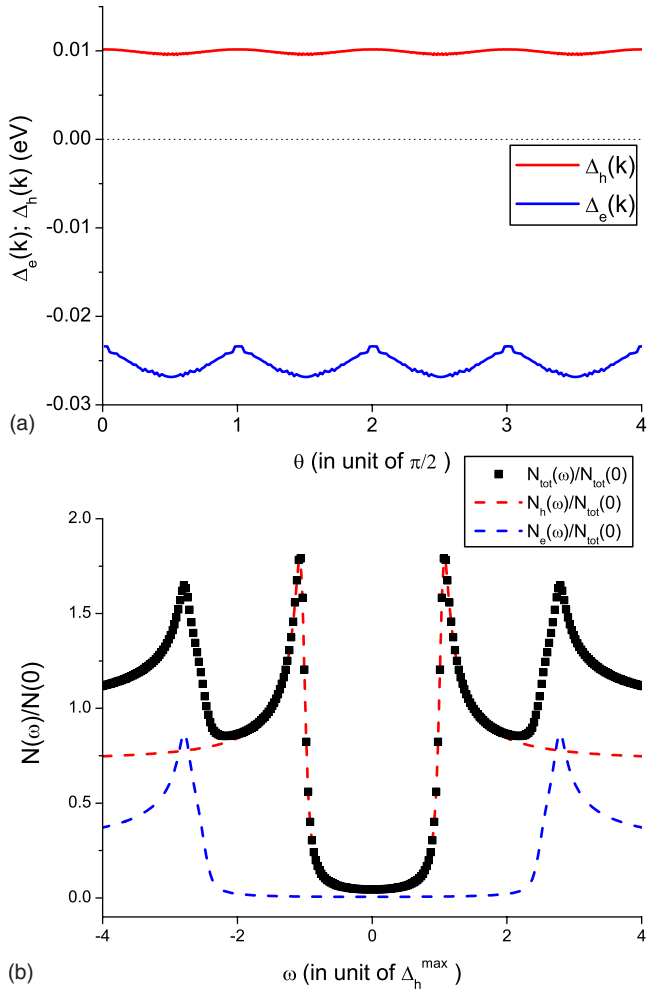

FIG. 2. (Color online) (a) $\pm s$-wave gap solutions $\Delta_h(k)$ and $\Delta_e(k)$. (b) Normalized DOS of the hole band $N_h(\omega)$ (red dotted line), electron band $N_e(\omega)$ (blue dotted line), and the total $N_{\text{tot}}(\omega)$ (solid black squares).

is indeed realized with a simple phenomenological interaction, which mimics an AFM spin fluctuations, on the minimal two-band model representing the Fe-based SC compounds.

As we described above, the reversed relation between the magnitude of the DOSs and the size of gaps holds more rigorously for the s-wave case and we suggest an approximate relation $\Delta_h^{\max} N_h \approx \Delta_e^{\max} N_e$ (see the Appendix for more detailed discussions). This relation is a generic feature of the model. Therefore, given a substantial difference of DOS between the hole and electron bands (several band calculations[3–8] indicate that this is true for the Fe-based SC materials), at least two distinctively different sizes of the SC gaps should be observed in various experiments.[23] In particular, because the band with a larger DOS would dominate the physical properties but actually holds a smaller gap, this feature will modify various SC properties of the Fe-based SC in unorthodox manner such as Δ/T_c value, temperature dependencies of various SC properties below T_c, and the responses to impurities.

In Fig. 2, the solution of the $\pm s$-wave gap and the corresponding DOS are shown. As mentioned, $N_h(0)=2.6N_e(0)$ for our bands. Accordingly the size of gaps of the hole band and the electron band is reversed as $\Delta_h^{\max} \approx 10$ meV and $\Delta_e^{\max} \approx 25$ meV. The strongly momentum-dependent pairing interaction and the realistic bands naturally induce an anisotropic modulation of the s-wave gaps with C_4 symmetry; the modulation is stronger for the larger gap on the smaller DOS band (electron band around M point). Compared to the case of the double d-wave solution, the average size of the $\pm s$-wave gap is larger by a factor of ~ 5 with the same pairing potential. Therefore, unless some other interactions are added, the ground state of our model is the $\pm s$-wave SC state. This conclusion is already obtained by other authors[5,17–19] with different models and approaches. The separate and total DOSs plotted in Fig. 2(b) show the main features of the $\pm s$-wave gap: two-peak structure, the large DOS with a small gap and the small DOS with a large gap. The overall shape of the total DOS is not very much revealing compared to the current tunneling DOS measurements.[10] However, it is too early to make a decisive conclusion with our calculations without including Andreev scattering. Also the ZBCP, the hallmark of a d-wave gap and observed in experiments with the Fe-based superconductors,[10] can equally be obtained with the $\pm s$-wave gap state.

We consider nuclear-spin-lattice relaxation rate $1/T_1$ for the $\pm s$-wave gap. Several groups[9,11] have reported that $1/T_1$ shows no coherence peak and the T^3 power law below T_c, strongly suggesting an unconventional gap with lines of node such as a d-wave gap. s-wave gap is known to have a constructive coherent factors for $1/T_1$ to induce the coherence peak over a temperature range below T_c. However, as Mazin *et al.*[5] envisaged, the sign-changing gaps between two bands provide a destructive coherent factor for the interband scattering which will largely cancel the intraband coherent factors. As a result the coherent peak of $1/T_1$ for the $\pm s$-wave gap SC will be substantially reduced. The explicit formula that we used for the calculations is the following:

$$\frac{1}{T_1} \sim -T\int_0^\infty \frac{\partial f_{\text{FD}}(\omega)}{\partial \omega}\left\{\left[N_h^2(0)\left\langle \text{Re}\frac{\omega}{\sqrt{\omega^2-\Delta_h^2(k)}}\right\rangle_k^2 + 2N_h(0)N_e(0)\times\left\langle \text{Re}\frac{\omega}{\sqrt{\omega^2-\Delta_h^2(k)}}\right\rangle_k\left\langle \text{Re}\frac{\omega}{\sqrt{\omega^2-\Delta_e^2(k')}}\right\rangle_{k'} + N_e^2(0)\times\left\langle \text{Re}\frac{\omega}{\sqrt{\omega^2-\Delta_e^2(k)}}\right\rangle_k^2\right] + \left[N_h^2(0)\left\langle \text{Re}\frac{\Delta_h(k)}{\sqrt{\omega^2-\Delta_h^2(k)}}\right\rangle_k^2 + 2N_h(0)N_e(0)\times\left\langle \text{Re}\frac{\Delta_h(k)}{\sqrt{\omega^2-\Delta_h^2(k)}}\right\rangle_k\left\langle \text{Re}\frac{\Delta_e(k')}{\sqrt{\omega^2-\Delta_e^2(k')}}\right\rangle_{k'} + N_e^2(0)\times\left\langle \text{Re}\frac{\Delta_e(k)}{\sqrt{\omega^2-\Delta_e^2(k)}}\right\rangle_k^2\right]\right\}. \quad (8)$$

For the temperature dependence of the gaps $\Delta_{h,e}(k,T)$, we use a phenomenological formula $\Delta_{h,e}(k,T)=\Delta_{h,e}(k,T=0)\tanh(\beta\sqrt{T_c/T-1})$. By choosing the values of $\Delta_{h,e}^{\max}/T_c$, we can partially take into account of the strong-coupling super-

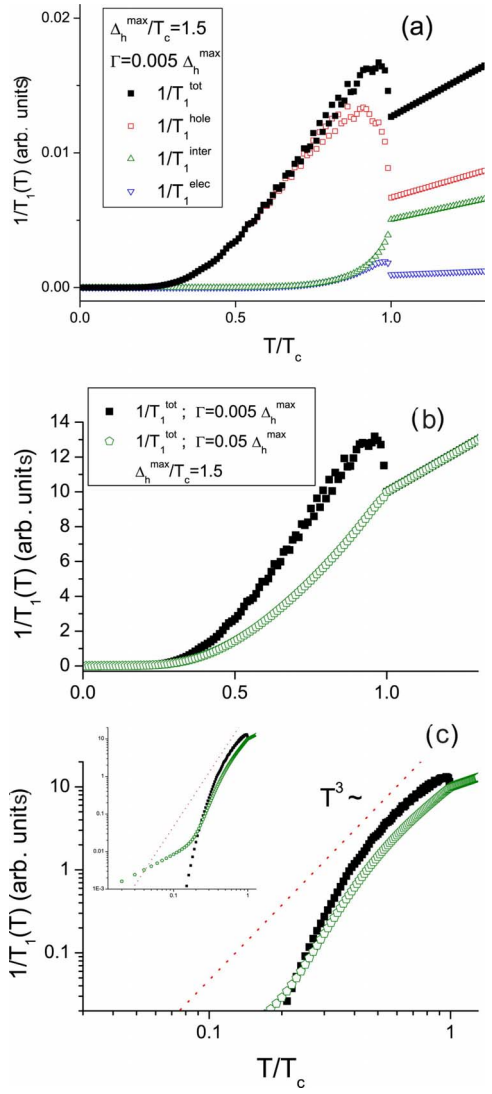

FIG. 3. (Color online) $1/T_1(T)$ of the $\pm s$-wave gap with $\Delta_h^{\max}/T_c=1.5$. (a) Separate term contributions of Eq. (8): total (solid black square), hole band (open red square), electron band (open blue triangle), and interband terms (solid green square). (b) Total $1/T_1(T)$ without (solid black square) and with (open green pentagon) damping. (c) The log-log plot of (b). The inset is a wide view.

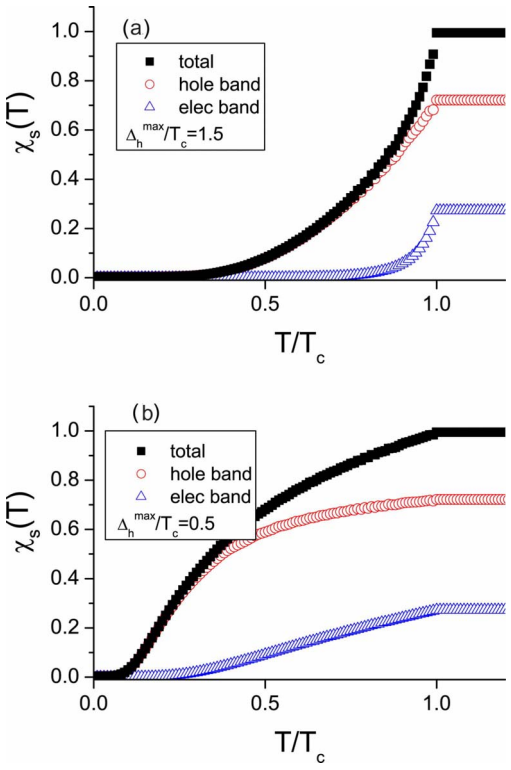

FIG. 4. (Color online) Normalized Knight shift (uniform spin susceptibility) of $\pm$s-wave gap. The total (solid black square), hole band (open red circle), and electron band (open blue triangle) contributions are shown separately. (a) $\Delta_h^{\max}/T_c=1.5$ and (b)$\Delta_h^{\max}/T_c=0.5$.

conductivity effect. β is not a sensitive parameter for final results; we take $\beta=1.74$ in this paper.

Figure 3(a) shows the contributions to the $1/T_1$ relaxation rate from each terms of Eq. (8): the hole band, the electron band, and the interband terms. It shows that the cancellation of the coherence factors is not perfect in general unless the conditions $N_h(0)=N_e(0)$ as well as $|\Delta_h(k)|=|\Delta_e(k)|$ are fulfilled. Nevertheless, due to the large cancellation by the interband coherence factor, the height of the coherence peak is very much reduced [compare the total $1/T_1$ and the hole band only $1/T_1$ in Fig. 3(a)]. Small amount of impurities can easily wash out this reduced coherence peak as shown in Fig. 3(b); the damping rate $\Gamma=0.05\Delta_h^{\max}$ is enough to completely kill the coherence peak. The subtle part is to fit the $\sim T^3$ power law below T_c. It requires to tune $R=\Delta_h^{\max}/T_c$ ratio. In Fig. 3, $R=1.5$ (automatically, it makes $\Delta_e^{\max}/T_c\approx 3.75$ which is quite a large value) is used for the best fit. Figure 3(c) shows that this pseudo-T^3 behavior is not extended to the very low-temperature region as in the d-wave case because this T^3 behavior in the $\pm$s-wave gap is not an intrinsic property of the lines of nodes. At low temperatures, there appears the exponential drop inevitably due to the full gaps, and then it finally reaches the impurity-induced T-linear region because we added some amount of impurities to kill the coherent peak. All these details put rather stringent conditions to confirm the $\pm s$-wave gap state with experiments.

Now we consider the Knight shift which is the measure of uniform susceptibility in SC phase. Because it is a $\mathbf{q}\rightarrow 0$ probe, there is no interband contribution and the total Knight shift is just sum of the contributions from each band as follows:

$$\chi_S(T) \sim -\int_0^\infty \frac{\partial f_{\mathrm{FD}}(\omega)}{\partial \omega}\left[N_h(0)\left\langle \mathrm{Re}\frac{\omega}{\sqrt{\omega^2-\Delta_h^2(k)}}\right\rangle_k + N_e(0)\times\left\langle \mathrm{Re}\frac{\omega}{\sqrt{\omega^2-\Delta_e^2(k)}}\right\rangle_k\right] \quad (9)$$

In Fig. 4, the normalized Knight shift (uniform spin susceptibility) is plotted and it shows the typical flat behavior of a s-wave gap at low temperatures. The contributions from the hole and electron bands show separately the feature of the larger DOS with small gap and the smaller DOS with a larger gap. Figure 4(a) is the results with $\Delta_h^{\max}/T_c=1.5$, the

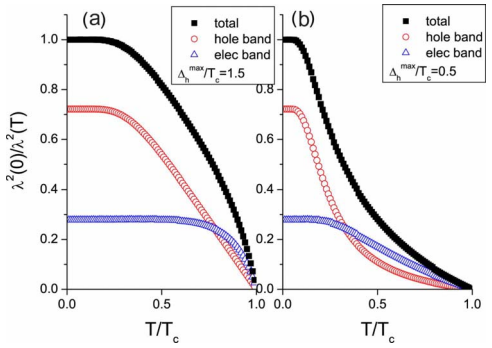

FIG. 5. (Color online) Normalized superfluidity density $\lambda^2(0)/\lambda^2(T)$ of $\pm s$-wave gap and its separate contributions from the hole and electron bands. (a) $\Delta_h^{\max}/T_c=1.5$ and (b)$\Delta_h^{\max}/T_c=0.5$.

best gap-T_c ratio to fit T^3 behavior of $1/T_1$ in Fig. 3. Figure 4(b) showed the results with $\Delta_h^{\max}/T_c=0.5$ to demonstrate the convex shape of Knight shift which was reported by Matano *et al.*[9] for Pr(FO)FeAs. Impurities do not change much of this feature unlike in the case of d-wave gap.

Finally, we consider the penetration depth. The static response function to the electromagnetic fields is the following:[24]

$$K_{h,e}(q,T)=2\pi T\sum_n\left\langle \hat{k}\|^2\frac{\Delta_{h,e}^2(k)}{\sqrt{\omega_n^2+\Delta_{h,e}^2(k)}[\omega_n^2+\Delta_{h,e}^2(k)+\alpha^2]}\right\rangle_k. \tag{10}$$

The $\mathbf{q}=0$ limit of this kernel $K(q=0,T)$ is directly proportional to the superfluidity density or $1/\lambda_L^2(T)$ in the London limit. For our two-band model, total kernel is the sum of $K_h(q,T)$ and $K_e(q,T)$ with the proper weighting factor proportional to the DOS $N_{h,e}(0)$ of each band and there is no interband screening current. $\alpha=(v_F/2)\hat{\mathbf{q}}\hat{\mathbf{k}}$ is the nonlocal parameter and can be rewritten in more convenient form as $\alpha=(\frac{\xi_0}{\lambda_0})\hat{\mathbf{q}}\hat{\mathbf{k}}$. $\xi_0\approx v_F/\Delta^{\max}$ and λ_0 are the coherence length and the penetration depth at zero temperature, respectively. Apparently if $(\frac{\xi_0}{\lambda_0})=\alpha_0$ is small compared to 1, the nonlocal effect becomes negligible. A typical value of α_0 for $YBa_2Cu_3O_{7-\delta}$ was estimated about 0.01, for example.[24] For the Fe-based superconductors, we believe that α_0 is not much larger than the values of high-T_c cuprates. Also for a s-wave case, the nonlocal effect does not change much of the temperature dependence of $1/\lambda^2(T)$ except the overall magnitude. Therefore, we take $\alpha_0=0.0$ for the calculations of the penetration depth in the $\pm s$-wave case. However, this effect can induce an important modifications in the d-wave case, which will be discussed in Sec. III B.

Figure 5 shows the normalized superfluidity density $\lambda^2(0)/\lambda^2(T)$ and separate contributions from the hole and electron bands. The exponentially flat region appears at low temperatures due to the full gap opening, which is consistent with recent experiments.[13] Relatively narrower region of the flat part (for $T<0.2T_c$) compared to the ordinary s-wave gap is another feature due to the smaller gap with the larger DOS of the $\pm s$-wave gap SC. A subtle part here is to fit the high-temperature region ($0.3T_c<T<T_c$). With $\Delta_h^{\max}/T_c=1.5$ (the same value used for the $1/T_1$ fit), this part becomes too convex [Fig. 5(a)] in comparison to the experiments.[13] A smaller gap-T_c ratio can make it concave as shown in Fig. 5(b) (with $\Delta_h^{\max}/T_c=0.5$); this concave feature was recently observed by Martin *et al.*[13]

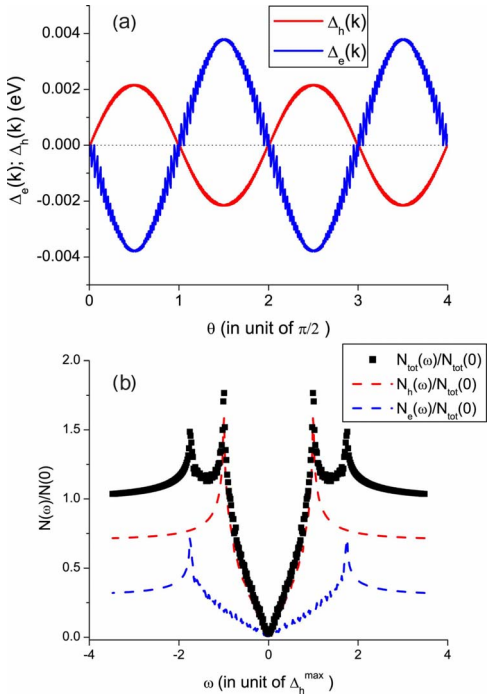

FIG. 6. (Color online) (a) Double d-wave gap solutions $\Delta_h(k)$ and $\Delta_e(k)$. (b) Normalized DOS of the hole band $N_h(\omega)$ (red dotted line), electron band $N_e(\omega)$ (blue dotted line), and the total $N_{\text{tot}}(\omega)$ (black squares).

In summary, the $\pm s$-wave gap state provides the most consistent descriptions for the penetration depth experiments. However, it explains $1/T_1$ only for a limited temperature range even with a fine tuning of $\Delta_{h,e}/T_c$ ratio and impurities. Knight shift of any shape can be fit with two-band parameter (this is also true with the double d-wave gap). The tunneling DOS does not provide a decisive conclusion.

B. Double d-wave gap

In Fig. 6, the gap solution and the corresponding DOS of the double d-wave gap are shown. As mentioned, our model bands have $N_h(0)=2.6N_e(0)$, and consequently gap in the hole band $\Delta_h^{\max}\approx 2$ meV is smaller than the one of the electron band $\Delta_e^{\max}\approx 4$ meV. The sizes of the maximum gaps are $\sim 5\times$ smaller than the $\pm s$-wave gap solutions. Therefore, the double d-wave gap solution is not the best SC state for our phenomenological model with an antiferromagnetic pairing interaction. This result is in agreement with other theoretical studies.[5,17,18] This conclusion may change with the correlation length of the AFM fluctuations, the sizes of the FS of the hole and electron bands, etc. But we numerically found that $\pm s$-wave gap solution is favored compared to the double d-wave gap solution for most cases. As discussed in Sec. II, however, the screened Coulomb interaction may

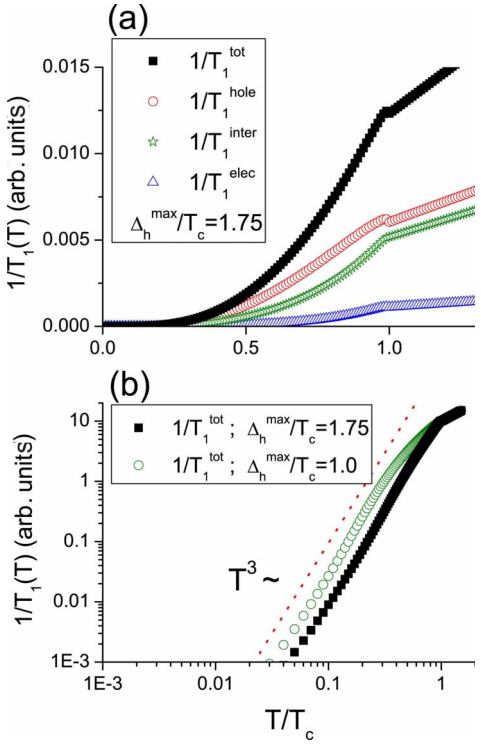

FIG. 7. (Color online) $1/T_1(T)$ of the double d-wave gap. (a) Each term contributions of Eq. (8): total (solid black square), hole band (open red square), electron band (open blue triangle), and interband terms (open green triangle). (b) Log-log plot of total $1/T_1(T)$ for $\Delta_h^{max}/T_c=1.75$ (black square) and 1.0 (green circle).

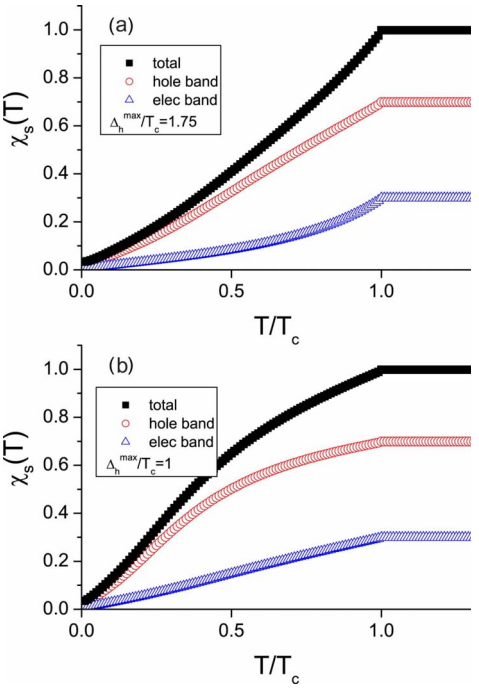

FIG. 8. (Color online) Normalized Knight shift (uniform spin susceptibility) of the double d-wave gap: the total (solid black square), the hole band (open red circle), and electron band (open blue triangle) contributions are shown separately. (a) $\Delta_h^{max}/T_c=1.75$ and (b) $\Delta_h^{max}/T_c=1.0$.

change this conclusion. The detailed studies about this issue will be discussed in a separate paper.

To complete the comparisons, we calculated the same SC properties of the double d-wave gap state. The separate and total DOSs shown in Fig. 6(b) demonstrate the main features of the double d-wave gap: the large DOS band with a small gap and the small DOS band with a large gap. This result shows a similar feature of the tunneling DOS measurement by Wang *et al.*[10] except the ZBCP, which does not show up in our simple DOS calculation but should appear when the tunneling conductivity is properly calculated with Andreev scattering process.

We consider the nuclear-spin-lattice relaxation rate $1/T_1$. As in the case of $\pm s$-wave gap, there are three contributions for the total $1/T_1$ relaxation rate: hole band, electron band, and interband scattering terms. The formula is the same as Eq. (8) but the last three terms should be dropped because the FS average of $\Delta_{h,e}(k)$ vanishes in this case. We use the same form of temperature-dependent gap function as $\Delta_{h,e}(k,T)=\Delta_{h,e}(k,T=0)\tanh(1.74\sqrt{T_c/T-1})$. In Fig. 7, $R=\Delta_h^{max}/T_c=1.75$ is used for the best T^3 fit below T_c. However, in the double d-wave gap, $R=1.5-2.5$ provide reasonably good fits, showing a more tolerance than the $\pm s$-wave gap state.

Figure 7(a) shows the separate contributions from each channel together with the total contribution. As in the $\pm s$-wave case, $1/T_{1,h}$ provides the largest contribution and $1/T_{1,e}$ provides the smallest contribution. There is also the interband term $1/T_1^{inter}$. In contrast to the $\pm s$-wave case, all three terms display a similar temperature dependence and no coherence peaks. Figure 7(b) shows the same $1/T_1^{total}$ (black squares) in log-log plot. The overall features of $1/T_1$ are the ones of the typical d-wave SC state: no coherence peak near T_c and $\sim T^3$ below T_c and consistent with the current NMR experiments.[9,11] At very low temperatures, T-linear behavior starts to appear due to a small damping for the numerical calculations ($\Gamma=0.005\Delta_h^{max}$). For comparison, we also show $1/T_1^{total}$ (open green circles) with $\Delta_h^{max}/T_c=1.0$, a smaller gap-T_c ratio; it exhibits a substantial convex part below T_c and then starts displaying the universal T^3 behavior before entering the impurity-dominating region.

In Fig. 8, we show the result of the uniform spin susceptibility which is measured as Knight shift. Figure 8(a) shows the results with $\Delta_h^{max}/T_c=1.75$. The hole band contribution is dominant as in $1/T_1$ and the electron band contribution show the steeper drop just below T_c because of the larger gap-T_c ratio $\Delta_e^{max}/T_c\approx 3.5$. The overall behavior of the total $\chi_s(T)$ below T_c shows a typical d-wave behavior such as T linear at low temperatures. Figure 8(b) shows the results with $\Delta_h^{max}/T_c=1.0$. A smaller gap-T_c ratio makes the Knight shift convex as in the $\pm s$-wave case and observed by Matano *et al.*[9] for Pr(FO)FeAS. This result demonstrates that this convex behavior of Knight shift is irrelevant to the gap symmetry but a generic feature of the two-gap (or multigap) SC. But it reveals that the gap-T_c ratio $\Delta^{max}(0)/T_c$ is much smaller than the standard BCS value, where $\Delta^{max}(0)$ refers to the gap of the band with largest DOS.

Now we calculate the penetration depth. As we discussed in Sec. II, most of experiments, up to now, report a flat tem-

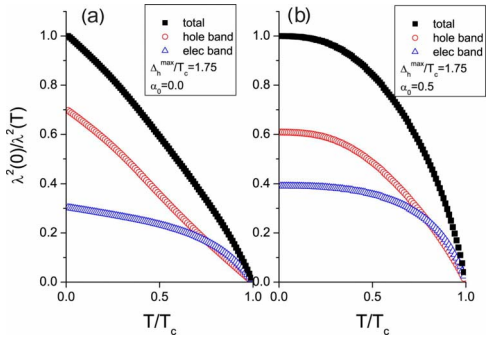

FIG. 9. (Color online) Normalized superfluidity density $\lambda^2(0)/\lambda^2(T)$ of double d-wave gap and its separate contributions from the hole and electron bands with $\Delta_h^{\max}/T_c=1.75$. (a) $\alpha_0=\frac{\xi_0}{\lambda_0}=0.0$ and (b) $\alpha_0=0.5$.

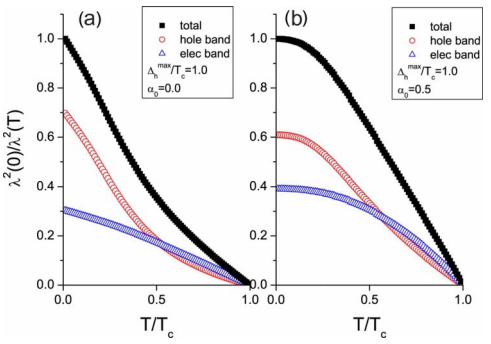

FIG. 10. (Color online) Normalized superfluidity density $\lambda^2(0)/\lambda^2(T)$ of double d-wave gap and its separate contributions from the hole and electron bands with $\Delta_h^{\max}/T_c=1.0$. (a) $\alpha_0=\frac{\xi_0}{\lambda_0}=0.0$ and (b) $\alpha_0=0.5$.

perature dependence of $\lambda(T)$ at low-temperature region and suggest a fully gapped SC state.[13] A naive double d-wave gap state has no chance to explain this flat behavior at low temperatures. Therefore, we consider a nonlocal effect of the electromagnetic response of the double d-wave gap superconductor as a possible cause to modify the typical temperature dependence. In order to include the effect of the nonlocal electrodynamics, we use the fully **q**-dependent kernel $K_{h,e}(q,T)$ [Eq. (10)] and put it into the integral formula for $\lambda(T)$ with the specular boundary condition

$$\frac{\lambda_{\rm spec}(T)}{\lambda_0}=\frac{2}{\pi}\int_0^\infty \frac{d\tilde{q}}{\tilde{q}^2+N_h(0)\tilde{K}_h(q,T)+N_e(0)\tilde{K}_e(q,T)}, \tag{11}$$

where $\tilde{K}_{h,e}(q,T)$ are the normalized kernels as $\tilde{K}_{h,e}(0,0)=1$ and $\tilde{q}=q\lambda_0$ is a dimensionless momentum. The results with a diffusive boundary condition are qualitatively the same; therefore, they will not be discussed. For the nonlocal parameter α_0, we think it to be much smaller than 1 for the Fe-based superconductors, but here we take it as a free parameter and see how large value is needed to fit experimental data.

Figures 9 and 10 show the normalized total superfluidity density $\lambda^2(0)/\lambda^2(T)$ and separate contributions from the hole and electron bands for the double d-wave gap state. Figure 9 used $\Delta_h^{\max}/T_c=1.75$ and Fig. 10 used $\Delta_h^{\max}/T_c=1.0$. In each figure, panel (a) is a local limit ($\alpha=0.0$) and the panel (b) is a nonlocal limit ($\alpha=0.5$). The local cases display the typical d-wave behavior at low temperatures, i.e., the linear decrease in T from $T=0$. The extreme nonlocal cases ($\alpha_0=\frac{\xi_0}{\lambda_0}=0.5$) introduce a substantial round-off ($\sim T^2$) region at low temperatures which is, however, not an exponentially flat behavior as the recent experiments claim. Further, even a rough fitting requires an unreasonably large nonlocal parameter α_0.

In summary, the double d-wave gap state can provide consistent descriptions for tunneling DOS, $1/T_1$, and Knight shift. However, there is an intrinsic difficulty to explain the flat behavior of the penetration depth at low temperatures. Also, in our model with an AFM mediated pairing interaction only, the double d-wave gap solution is energetically less favored than the $\pm s$-wave gap solution.

IV. CONCLUSION

We demonstrated that a minimal model with a phenomenological pairing interaction of the AFM spin fluctuations can allow both the $\pm s$-wave gap and the double d-wave gap solutions with the realistic bands of the Fe-based SC compounds. With the same parameters, the $\pm s$-wave gap solution is energetically more favorable by a factor of $\sim 5\times$, so that it has a better chance to be realized in the Fe-based SC compounds.

In both cases, we found that the approximate relation $\Delta_h^{\max}N_h \approx \Delta_e^{\max}N_e$ holds because it is a generic feature of the two-gap SC when an interband pair scattering is the dominant pairing interaction. This relation appears for all SC properties in subtle way, which modifies the value of $\Delta(0)/T_c$ and other SC properties in unorthodox way. Numerically solving the coupled gap equations for the two bands, we found the detailed structure of the gap functions $\Delta_{h,e}(k)$, which showed an anisotropy ($\sim 20\%$) of the $\pm s$-wave gaps. We also calculated the key SC properties for both gap states such as tunneling DOS, $1/T_1$, Knight shift, and penetration depth and discussed them in comparison with experiments. When we calculated these quantities, we paid special attention to the interband coherence factor which is a unique feature of multigap SC. This interband coherence factor particularly produced an important modification to the $1/T_1$ relaxation rate of the $\pm s$-wave gap state.

The $\pm s$-wave gap state provides the most consistent descriptions for the penetration depth experiments: the flat low-temperature behavior.[13] Besides the low-temperature behavior, the high-temperature ($0.3T_c<T<T_c$) behavior—due to a large difference of the gap sizes Δ_h and Δ_e and their corresponding DOS $N_{h,e}$—can be either concave or convex. However, $1/T_1$ experiments can only be fitted for a limited temperature range even with a fine tuning of $\Delta_{h,e}/T_c$ ratio and impurities. The $\pm s$-wave gap state is not inconsistent with the Knight shift and the tunneling DOS data but overall does not provide any decisive merit in comparison with the double d-wave gap.

The double d-wave gap state, although it is energetically less favorable in our model unless additional interactions are added, provides the best fit to the $1/T_1$ experiments. However, it has a difficulty to explain the penetration depth experiments for the low-temperature flat behavior. It requires an unreasonably large nonlocal effect to fit the low-temperature part; it is still not exponentially flat but only $\sim T^2$. If this low-temperature part of $\lambda(T)$ is, indeed, confirmed to be exponentially flat, the double d-wave gap state should be ruled out. Tunneling DOS and Knight shift can be fit with the double d-wave gap state as much as with the $\pm s$-wave gap state.

In conclusion, quantitative calculations carried out in this paper, with the two most promising SC gap states, can serve as guidelines for sorting out the possible pairing states of the Fe-based SC in comparison with the current and future experiments. For that, very low-temperature measurements and systematic studies with the amount of impurities will provide decisive information to determine the correct gap symmetry.

Note added. Recently, we have known that similar studies of $1/T_1$ for the $\pm s$-wave state were carried out by two groups[25] where only the interband scattering process was analyzed and by another recent paper[26] where both the interband and intraband processes were considered as in our paper.

ACKNOWLEDGMENTS

This work was supported by the KOSEF through Grants No. KRF-2007-070-C00044 and No. KRF-2007-521-C00081.

APPENDIX: RELATION BETWEEN Δ_h/Δ_e AND N_h/N_e

In the main text, we claimed the approximate relation $N_h\Delta_h \approx N_e\Delta_e$ as a generic feature of the two-band model with a dominant interband interaction. This kind of relation will have direct and important implications to the experimental observations. However it is pointed out by Mazin[27] that this is not a rigorous identity in general. In this appendix, we clarify the degree of the validity of this relation.

Here we consider the $\pm s$-wave gap state only. Assuming constant gaps $\Delta_h(k)=\Delta_h$ and $\Delta_e(k)=-\Delta_e$ and only the interband interaction, the coupled gap equations (5) and (6) are simplified as

$$\Delta_h = V_{he}\Delta_e\chi_e(T,\Delta_e,\omega_{\mathrm{AFM}}), \tag{A1}$$

$$\Delta_e = V_{eh}\Delta_h\chi_h(T,\Delta_h,\omega_{\mathrm{AFM}}), \tag{A2}$$

where χ_h and χ_e are defined with Eq. (7).

First, when $T=T_c$, the above equations can be written as

$$\Delta_h = V_{he}N_e\Delta_e \times \mathrm{const}, \tag{A3}$$

$$\Delta_e = V_{eh}N_h\Delta_h \times \mathrm{const}, \tag{A4}$$

where $\mathrm{const}=\int_0^{\omega_{\mathrm{AFM}}} d\xi \frac{\tanh(\xi/2T_c)}{\xi} \approx \log 1.14\omega_{\mathrm{AFM}}/T_c$. Because $V_{he}=V_{eh}$, we immediately obtain the following relation from the above equations:

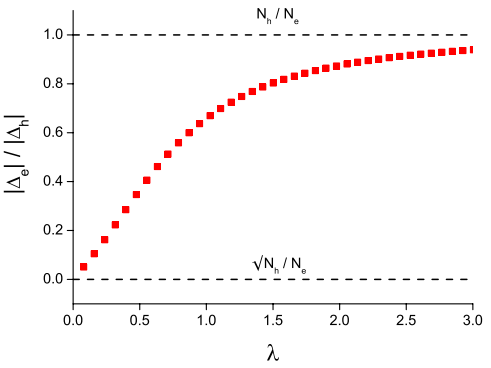

FIG. 11. (Color online) Normalized gap ratio $|\Delta_e|/|\Delta_h|$ vs the dimensionless coupling constant $\lambda=\sqrt{V_{he}V_{eh}N_hN_e}$. The bottom baseline is $\sqrt{N_h/N_e}$ and the top baseline is N_h/N_e.

$$\frac{\Delta_e}{\Delta_h} = \sqrt{\frac{N_h}{N_e}}, \quad T=T_c. \tag{A5}$$

Next, when $T=0$, Eqs. (A1) and (A2) are written as

$$\Delta_h = V_{he}N_e\Delta_e \log\left(\frac{\omega_{\mathrm{AFM}}+\sqrt{\omega_{\mathrm{AFM}}^2+\Delta_e^2}}{\Delta_e}\right), \tag{A6}$$

$$\Delta_e = V_{eh}N_h\Delta_h \log\left(\frac{\omega_{\mathrm{AFM}}+\sqrt{\omega_{\mathrm{AFM}}^2+\Delta_h^2}}{\Delta_h}\right). \tag{A7}$$

In general, these equations do not yield a simple algebraic relation between Δ_e/Δ_h and N_h/N_e, but we can obtain the simple relations for the limiting cases. First, for the extreme weak-coupling limit, i.e., when $\Delta_{h,e} \ll \omega_{\mathrm{AFM}}$, the two logarithmic terms become asymptotically equal as $\log(2\omega_{\mathrm{AFM}}/\Delta_e) \approx \log(2\omega_{\mathrm{AFM}}/\Delta_h)$, and we obtain the same relation as the $T=T_c$ case (A5). On the other hand, for strong-coupling limit, i.e., when $\Delta_{h,e} \gg \omega_{\mathrm{AFM}}$ (which is certainly an unphysical limit), $\log[(\omega_{\mathrm{AFM}}+\sqrt{\omega_{\mathrm{AFM}}^2+\Delta_{h,e}^2})/\Delta_{h,e}] \approx \omega_{\mathrm{AFM}}/\Delta_{h,e}$ and we obtain the relation

$$\frac{\Delta_e}{\Delta_h} = \frac{N_h}{N_e}, \quad T=0, \quad \Delta_{h,e} \gg \omega_{\mathrm{AFM}}. \tag{A8}$$

Having found the results of the two limiting cases, we can guess that the gap ratio Δ_e/Δ_h should be in between these two limiting ratios. For example, we can attempt an expansion with $x=\log[N_h/N_e]$ starting from the weak-coupling limit[27] and we obtain, in the first order of x,

$$\frac{\Delta_e}{\Delta_h} \approx \sqrt{\frac{N_h}{N_e}}\left(1+\frac{\log[N_h/N_e]}{4}\lambda+\ldots\right), \tag{A9}$$

where $\lambda=\sqrt{V_{he}V_{eh}N_hN_e}$ is a dimensionless coupling constant. For practical use, we numerically solve Eqs. (A1) and (A2) and plot the ratio Δ_e/Δ_h as a function of λ in Fig. 11. The ratio Δ_e/Δ_h becomes a universal curve when it is normalized by the distance between $\sqrt{\frac{N_h}{N_e}}$ and $\frac{N_h}{N_e}$. The result indeed shows that when $\lambda \approx 1$, it is in between two limiting ratios $\sqrt{\frac{N_h}{N_e}}$ and $\frac{N_h}{N_e}$ as we expected from the above analysis.

In reality, there exist two complications. First, the intraband couplings V_{hh} and V_{ee} need to be included. A little analysis of Eqs. (5) and (6) as well as of numerical results reveals that this effect always enhances the gap ratio toward the limit $\frac{N_h}{N_e}$. Another complication arises from the fact that there are more than two bands in real materials.[3–8] Applying the results of the above analysis, we can suggest the following approximate relations. First, we classify the bands of the real materials into two groups: the hole bands around Γ point and the electron bands around *M* point, respectively. Then in the strong-coupling limit,

$$\sum_i \Delta_{h,i} N_{h,i} \approx \sum_i \Delta_{e,i} N_{e,i}, \tag{A10}$$

and in the extreme weak-coupling limit,

$$\sum_i \Delta_{h,i} \sqrt{N_{h,i}} \approx \sum_i \Delta_{e,i} \sqrt{N_{e,i}}. \tag{A11}$$

Considering several uncertainties in reality, Eq. (A10) can serve as a practical rule of the thumb.

*Author to whom the correspondence should be addressed; ykbang@chonnam.ac.kr

[1] Y. Kamihara *et al.*, J. Am. Chem. Soc. **128**, 10012 (2006); **130**, 3296 (2008).
[2] G. F. Chen, Z. Li, D. Wu, G. Li, W. Z. Hu, J. Dong, P. Zheng, J. L. Luo, and N. L. Wang, Phys. Rev. Lett. **100**, 247002 (2008); X. H. Chen, T. Wu, G. Wu, R. Liu, H. Chen, and D. Fang, Nature (London) **453**, 761 (2008); Z. Ren *et al.*, Chin. Phys. Lett. **25**, 2215 (2008).
[3] D. J. Singh and M.-H. Du, Phys. Rev. Lett. **100**, 237003 (2008).
[4] K. Haule, J. H. Shim, and G. Kotliar, Phys. Rev. Lett. **100**, 226402 (2008).
[5] I. I. Mazin, D. J. Singh, M. D. Johannes, and M. H. Du, Phys. Rev. Lett. **101**, 057003 (2008).
[6] C. Cao, P. J. Hirschfeld, and H. P. Cheng, Phys. Rev. B **77**, 220506(R) (2008).
[7] E. Manousakis, Jun Ren, and E. Kaxiras, arXiv:0806.3432 (unpublished); D. Lu, M. Yi, S. Mo, A. Erickson, J. Analytis, J. Chu, D. Singh, Z. Hussain, T. Geballe, I. Fisher, and Z. Shen, arXiv:0807.2009 (unpublished).
[8] I. I. Mazin, M. D. Johannes, L. Boeri, K. Koepernik, and D. J. Singh, Phys. Rev. B **78**, 085104 (2008).
[9] K. Matano *et al.*, Europhys. Lett. **83**, 57001 (2008); H. Grafe, D. Paar, G. Lang, N. Curro, G. Behr, J. Werner, J. Hamannborrero, C. Hess, N. Leps, R. Klingeler, and B. Buechner, Phys. Rev. Lett. **101**, 047003 (2008).
[10] T. Y. Chen, Z. Tesanovic, R. H. Liu, X. H. Chen, and C. L. Chien, Nature (London) **453**, 1224 (2008); Y. Wang, L. Shan, L. Fang, P. Cheng, C. Ren, and H. Wen, arXiv:0806.1986 (unpublished); L. Shan, Y. Wang, X. Zhu, G. Mu, L. Fang, C. Ren, and H. Wen, Europhys. Lett. **83**, 57004 (2008).
[11] H. Mukuda, N. Terasaki, H. Kinouchi, M. Yashima, Y. Kitaoka, S. Suzuki, S. Miyasaka, S. Tajima, K. Miyazawa, P. Shirage, H. Kito, H. Eisaki, and A. Iyo, arXiv:0806.3238, J. Phys. Soc. Jpn. (to be published); Y. Nakai, K. Ishida, Y. Kamihara, M. Hirano, and H. Hosono, arXiv:0804.4765, J. Phys. Soc. Jpn. (to be published).
[12] G. Mu, X. Zhu, L. Fang, L. Shan, C. Ren, and H. Wen, Chin. Phys. Lett. **25**, 2221 (2008).
[13] L. Malone, J. Fletcher, A. Serafin, A. Carrington, N. Zhigadlo, Z. Bukowski, S. Katrych, and J. Karpinski, arXiv:0806.3908 (unpublished); K. Hashimoto, T. Shibauchi, T. Kato, K. Ikada, R. Okazaki, H. Shishido, M. Ishikado, H. Kito, A. Iyo, H. Eisaki, S. Shamoto, and Y. Matsuda, arXiv:0806.3149 (unpublished); C. Martin, R. Gordon, M. Tanatar, M. Vannette, M. Tillman, E. Mun, P. Canfield, V. Kogan, G. Samolyuk, J. Schmalian, and R. Prozorov, arXiv:0807.0876 (unpublished).
[14] L. Boeri, O. V. Dolgov, and A. A. Golubov, Phys. Rev. Lett. **101**, 026403 (2008).
[15] C. de la Cruz *et al.*, Nature (London) **453**, 899 (2008); J. Zhao, Q. Huang, C. Delacruz, S. Li, J. Lynn, Y. Chen, M. Green, G. Chen, G. Li, Z. Li, J. Luo, N. Wang, and P. Dai, arXiv:0806.2528 (unpublished).
[16] N. J. Curro, T. Caldwell, E. D. Bauer, L. A. Morales, M. J. Graf, Y. Bang, A. V. Balatsky, J. D. Thompson, and J. L. Sarrao, Nature (London) **434**, 622 (2005).
[17] F. Wang, H. Zhai, Y. Ran, A. Vishwanath, and Dung-Hai Lee, arXiv:0805.3343 (unpublished).
[18] M. M. Korshunov and I. Eremin, arXiv:0804.1793 (unpublished).
[19] K. Kuroki, S. Onari, R. Arita, H. Usui, Y. Tanaka, H. Kontani, and H. Aoki, Phys. Rev. Lett. **101**, 087004 (2008).
[20] Q. Han, Y. Chen, and Z. D. Wang, Europhys. Lett. **82**, 37007 (2008); Tao Li, arXiv:0804.0536 (unpublished); V. Cvetkovic and Z. Tesanovic, arXiv:0804.4678 (unpublished); G. Baskaran, arXiv:0804.1341 (unpublished); P. A. Lee and Xiao-Gang Wen, arXiv:0804.1739 (unpublished); X. Dai, Z. Fang, Yi Zhou, and Fu-chun Zhang, arXiv:0803.3982 (unpublished).
[21] A. D. Christianson *et al.*, arXiv:08047.3932 (unpublished).
[22] J. Dong, H. Zhang, G. Xu, Z. Li, G. Li, W. Hu, D. Wu, G. Chen, X. Dai, J. Luo, Z. Fang, and N. Wang, Europhys. Lett. **83**, 27006 (2008).
[23] H. Ding *et al.*, Europhys. Lett. **83**, 47001 (2008).
[24] I. Kosztin and A. J. Leggett, Phys. Rev. Lett. **79**, 135 (1997).
[25] D. Parker, O. V. Dolgov, M. M. Korshunov, A. A. Golubov, and I. I. Mazin, arXiv:0807.3729 (unpublished); A. V. Chubukov, D. Efremov, and I. Eremin, arXiv:0807.3735 (unpublished).
[26] M. M. Parish, J. Hu, and B. A. Bernevig, arXiv:0807.4572 (unpublished).
[27] This appendix section is motivated by the communication with I. I. Mazin and a large part of the analysis is directly suggested by him.